Effects of three-body forces on the maximum mass of neutron stars in the lowest-order constrained variational formalism

S. Goudarzi and H. R. Moshfegh
Department of Physics, University of Tehran, P.O.B 14395-547, Tehran, Iran
(Received 17 January 2015; revised manuscript received 15 April 2015; published 20 May 2015)

The equation of state of neutron star matter is calculated within the lowest order constrained variational (LOCV) method using different two-body interactions and an Urbana type three-body force. The core of the neutron star is modelled by β-stable matter. The corresponding neutron star mass-radius relations are presented and the effect of using a three-body interaction on the maximum gravitational mass of the star is also discussed. It is shown that including the three-body force generally increases the maximum gravitational mass.

DOI: 10.1103/PhysRevC.91.054320 PACS number(s): 26.60.−c, 24.10.Cn, 21.65.Mn, 97.60.Jd

I. INTRODUCTION

Neutron stars (NSs) are compact objects supported by degenerate-neutron pressure which were born as a result of the gravitational collapse of the iron core of massive stars in a type-II supernova [1]. Some minutes after birth, the temperature throughout the NS is less than 1 MeV and the thermal effects are negligibly small [2]. Therefore neutron stars can be used as astrophysical environments for testing theories of cold and dense matter. The existence of massive neutron stars has been recently reported. One remarkable example is the radio pulsar J1614-2230 with a mass of $M = 1.97 \pm 0.04 M_\odot$ [3]. The other one is J0348+0432 with $M = 2.01 \pm 0.04 M_\odot$ [4]. According to recent analysis [5,6] radii of $0.8 M_\odot$ to $2.0 M_\odot$ neutron stars are ranged from 10.9 to 12.8 km. In order to determine the structure of neutron stars, the equation of state (EOS) of NS matter over a wide range of densities is required. For any given EOS, there is a maximum mass a neutron star can have. All acceptable EOS should generate mass-radius relations which are in agreement with the empirical restrictions on neutron star radii and masses. Therefore theoretical study of the NS matter is fundamentally important in neutron star modeling.

There are some reliable many-body approaches that have been used for studying nuclear matter as well as neutron star structure. Theoretical methods such as Brueckner-Hartree-Fock (BHF) [7,8], Dirac-BHF [9,10], variational [11,12], and Monte Carlo [13–15] methods are among them. In the present work we use the lowest order constrained variational (LOCV) approach for determining the EOS of a neutron star.

The LOCV method was presented in a series of papers [16,17] to calculate the properties of nuclear matter at zero temperature for the Reid-type potentials [18,19]. Later on, this method was developed for finite temperature calculations [20] and also for determining various thermodynamic properties of different nuclear systems such as symmetric and asymmetric nuclear matter [21,22], neutron matter [23], and β-stable matter [24] using more sophisticated interactions [25] such as AV14 [26], AV18 [27], and UV14 [28]. This technique has also been generalized to include relativistic corrections in calculating thermodynamic properties of nuclear matter at both zero [29] and finite temperature [30]. The LOCV method is also fully self-consistent which means that no free parameter is considered in its formalism. Moreover, there is a constraint in this approach in the form of normalization condition [31,32] to keep the higher cluster terms small. Mentioned features are two valuable advantages of the LOCV method compared to other many-body techniques.

One important point that must be considered in studying the neutron star structure is the crucial role of three-body forces (TBF) at very high densities. On the other hand, like other theoretical approaches, the LOCV formalism is unable to produce the correct empirical saturation properties of cold symmetric nuclear matter if only two-body interactions are included in the Hamiltonian. In this work we intend to correct this deficiency and take into account the role of TBF at supernuclear densities by adding three-body forces to the nuclear matter Hamiltonian. To do this task we use the phenomenological Urbana-type (UIX) three-body force [13,33] and by adopting it in our method we discuss the procedure of adding this force to the former LOCV formalism. Therefore studying the effect of using three-body forces in the LOCV method is one of our aims in this work as well as discussing the role played by TBF in determining the mass-radius relation of neutron stars.

In view of the above, in the present work we study the mass-radius relation of cold neutron stars. The star is assumed to be in β-equilibrium during its lifetime, i.e., it is composed of an uncharged mixture of neutrons, protons, electrons, and muons in equilibrium with respect to the weak interaction. We construct the EOS for the above system by using the LOCV method with different nucleon-nucleon potentials such as AV18, AV14, UV14, and Reid68 [18].

The structure of the article is as follows. In Sec. II we present our formalism based on the LOCV model for nuclear matter and β-stable matter at zero temperature. In Sec. III we briefly review the UIX three-body force model and describe combining TBF with the two-body interaction in our method. Results and discussion are presented in Sec. IV. Finally the conclusion is given in Sec. V.

II. THE LOCV FORMALISM

In this section we briefly review the lowest order constrained variational method. First we restrict our attention to baryonic matter and at the next stage we apply this formalism to determine the EOS of stellar matter in β-equilibrium.

A. Asymmetric matter

In the LOCV method we use a trial wave function for the many-body interacting system which can be written as follows [24]:

$$\Psi(1\dots A) = F(1\dots A)\Phi(1\dots A), \tag{1}$$

where Φ represents the uncorrelated ground state wave function, simply the Slater determinant of plane waves, and F is an A-body correlation operator which is defined as the product of two-body correlation function operators, i.e.,

$$F = S\prod_{i>j} f(ij), \tag{2}$$

where S is the symmetrizing operator. $f(ij)$ are written as

$$f(ij) = \sum_{\alpha,p=1}^{3} f_\alpha^p(ij)O_\alpha^p(ij), \tag{3}$$

where $\alpha = \{J,L,S,T,T_z\}$ and p=1, 2, and 3. For singlet and triplet channels with $J = L$ we choose $p = 1$ and for triplet channels with $J = L \pm 1$ we set $p = 2$ and 3. The operators $O_\alpha^p(ij)$ are written as

$$O_\alpha^{p=1-3} = 1, \left(\tfrac{2}{3} + \tfrac{1}{6}S_{12}\right), \left(\tfrac{1}{3} - \tfrac{1}{6}S_{12}\right), \tag{4}$$

where $S_{12} = 3(\sigma_1\cdot\hat{r})(\sigma_2\cdot\hat{r}) - \sigma_1\cdot\sigma_2$ is the usual tensor operator. At this stage a cluster expansion for the expectation value of the nuclear Hamiltonian can be constructed by using the trial wave function. The Hamiltonian has the general form of

$$H = \sum_i \frac{p_i^2}{2m} + \sum_{i<j} V(ij), \tag{5}$$

where $V(ij)$ is a two-nucleon potential. In the cluster expansion series [34] we keep only the first two terms of the energy functional,

$$E[f] = \frac{1}{A}\frac{\langle\Psi|H|\Psi\rangle}{\langle\Psi\mid\Psi\rangle} = E_1 + E_{MB} \cong E_1 + E_2, \tag{6}$$

where A is total number of particles. The one-body term E_1 is independent of $f(ij)$ and is simply the Fermi-gas kinetic energy for asymmetrical nuclear matter,

$$E_1 = \sum_i \frac{3\hbar^2 k_{f_i}^2}{10m_i}. \tag{7}$$

While the two-body energy is defined as

$$E_2 = \frac{1}{2A}\sum_{ij}\langle ij|W(12)|ij-ji\rangle, \tag{8}$$

and

$$W(12) = -\frac{\hbar^2}{2m}\left[f(12),\left[\nabla_{12}^2, f(12)\right]\right] + f(12)V(12)f(12). \tag{9}$$

The two-body matrix elements $\langle ij|W(12)|ij-ji\rangle$ are calculated by using plane waves. Now by inserting a complete set of two-particle states twice in Eq. (8) and doing some algebra we arrive at the final expression for the two-body cluster energy. This expression is then minimized with respect to variations in the functions f_α^p but subject to the normalization constraint which is designed to ensure the rapid convergence of the cluster expansion [31,32,35]. The constraint which is employed is

$$\frac{1}{A}\sum_{ij}\langle ij|h_{T_z}^2(12) - f^2(12)|ij-ji\rangle = 0, \tag{10}$$

where $h_{T_z}(r)$ is the modified Pauli function which for the asymmetric nuclear matter takes the following form:

$$h_{T_z}(r) = \left[1 - \frac{9}{2}\left(\frac{J_1(k_i^F r)}{k_i^F r}\right)^2\right]^{-\frac{1}{2}}, \quad T_z = \pm 1$$
$$= 1, \quad T_z = 0, \tag{11}$$

where $J_L(x)$ is the spherical Bessel function of order L. The constraint given in Eq. (10) introduces a Lagrange multiplier λ. By minimizing the two-body cluster energy we get coupled and uncoupled Euler-Lagrange differential equations depending on the two-body potential we use. The reader is referred to the mentioned references for more detail.

B. β-stable matter

By assuming the neutron star as an object which is made of only neutrons, one can calculate the equation of state of such star by using Eq. (6). On the other hand it is well known that the presence of leptons is also crucial since the star matter has to be equilibrated against the weak leptonic decay. Thus we consider the NS as an object in which its matter contains neutrons, protons, electrons, and muons. τ lepton is ignored because of its large rest mass with respect to two other leptons. For such matter the β- equilibrium conditions without trapped neutrinos are

$$\mu_n = \mu_p + \mu_e, \tag{12}$$
$$\mu_e = \mu_\mu, \tag{13}$$

where μ_i indicates the chemical potential of each particle. At zero temperature the chemical potentials of leptons are their Fermi energy and can be expressed as

$$\mu_i = \sqrt{(p_{F,i}c)^2 + (m_i c^2)^2}. \tag{14}$$

On the other hand the charge neutrality condition in NS matter requires the following equality:

$$\rho_p = \rho_\mu + \rho_e. \tag{15}$$

By solving the coupled Eqs. (12), (13), and (15) self-consistently at a given baryon density ($\rho_B = \rho_n + \rho_p$), the energy of β-stable matter which is written as the sum of the baryonic part energy E_B and leptonic part energy E_L can be determined:

$$E = E_B + E_L. \tag{16}$$

The energy of baryonic part is calculated by using Eq. (6). Leptons are supposed to be noninteracting highly relativistic particles. Therefore at zero temperature the energy of leptonic

part can be written as

$$E_L = \frac{2}{h^3\rho_B}\sum_{l=e,\mu}\int_0^{p_{F_l}} d^3p_l\sqrt{(p_lc)^2+(m_lc^2)^2}, \tag{17}$$

which can be calculated analytically. By introducing $\phi_l = \frac{p_{F_l}}{m_lc}$, E_L takes the final following form:

$$E_L = \sum_{l=e,\mu}\frac{\pi c^5 m_l^4}{h^3\rho_B}\left[\phi_l\left(2\phi_l^2+1\right)\sqrt{\phi_l^2+1}-\sinh^{-1}\phi_l\right]. \tag{18}$$

It is clear that there is no muon in NS matter if $\mu_e < m_\mu c^2$. Equation (12) is satisfied by minimizing the total mass energy of the system with respect to proton density ρ_p. At this stage the pressure of NS matter as a function of baryon density can be determined by using the following relation:

$$P = \rho_B^2\frac{\partial(E/\rho_B)}{\partial\rho_B}. \tag{19}$$

III. THREE-BODY FORCE

As we mentioned before, three-body forces are included in our nuclear Hamiltonian for the purpose of reproducing the empirical saturation properties of cold asymmetric nuclear matter. We use the UIX interaction which is based on meson-exchange theory and is generally written as

$$V_{123} = V_{123}^{2\pi} + V_{123}^{R}. \tag{20}$$

The two-pion exchange contribution is written as [13]

$$V_{123}^{2\pi} = A\sum_{\text{cyc}}\Big(\{X_{12},X_{23}\}\{\tau_1.\tau_2,\tau_2.\tau_3\} + \frac{1}{4}[X_{12},X_{23}][\tau_1.\tau_2,\tau_2.\tau_3]\Big), \tag{21}$$

where

$$X_{12} = Y(m_\pi r_{12})\sigma_1.\sigma_2 + T(m_\pi r_{12})S_{12} \tag{22}$$

is the one-pion exchange operator. 1, 2, and 3 indices stand for three interacting nucleons. σ and τ are the Pauli spin and isospin operators and S_{12} is the usual tensor operator. m_π indicates the average pion mass and $Y(m_\pi r)$ and $T(m_\pi r)$ are the Yukawa and tensor functions, respectively, which are written as

$$Y(m_\pi r) = \frac{e^{-m_\pi r}}{m_\pi r}\left(1-e^{-cr^2}\right), \tag{23a}$$

$$T(m_\pi r) = \left(1+\frac{3}{m_\pi r}+\frac{3}{(m_\pi r)^2}\right)\frac{e^{-m_\pi r}}{m_\pi r}\left(1-e^{-cr^2}\right)^2, \tag{23b}$$

with $c = 2.1\,\text{fm}^{-2}$ [13,27]. The shorter-range part of V_{123} is a phenomenological one and has the form of [13]

$$V_{123}^{R} = U\sum_{\text{cyc}} T(m_\pi r_{12})^2 T(m_\pi r_{23})^2. \tag{24}$$

The strengths A and U in Eqs. (21) and (24) are determined in such a way that the resulting EOS will be able to reproduce the correct saturation properties of symmetric nuclear matter at zero temperature. By averaging over the third particle coordinates we reach to a reduced TBF [36], namely a density dependent effective two-body interaction $\bar{V}_{12}(r)$ being weighted by the LOCV two-body correlation functions $f(r)$ at each density:

$$\bar{V}_{12}(r) = \rho\int d^3r_3\sum_{\sigma_3,\tau_3} f^2(r_{13})f^2(r_{23})V_{123}. \tag{25}$$

By inserting Eq. (20) in the above relation, one can get an effective two-body potential which has the following operator structure:

$$\bar{V}_{12}(r) = (\tau_1.\tau_2)(\sigma_1.\sigma_2)V_{\sigma\tau}^{2\pi}(r) + S_{12}(\hat{r})(\tau_1.\tau_2)V_t^{2\pi}(r) + V_c^R(r), \tag{26}$$

where

$$V_{\sigma\tau}^{2\pi}(r) = \frac{2\pi}{r}\rho\int_0^\infty xdx\int_{|r-x|}^{|r+x|} ydyf^2(x)f^2(y) \times\sum_{\text{cyc}}\sum_{\sigma_3\tau_3}4A\times[Y(m_\pi x)Y(m_\pi y) + 2P_2(\cos\theta)T(m_\pi x)T(m_\pi y)], \tag{27a}$$

$$V_t^{2\pi}(r) = \frac{2\pi}{r}\rho\int_0^\infty xdx\int_{|r-x|}^{|r+x|} ydyf^2(x)f^2(y) \times\sum_{\text{cyc}}\sum_{\sigma_3\tau_3}4A\times[Y(m_\pi x)T(m_\pi y)P_2(\cos\theta_x) + T(m_\pi x)Y(m_\pi y)P_2(\cos\theta_y) + T(m_\pi x)T(m_\pi y)P], \tag{27b}$$

$$V_c^R(r) = \frac{2\pi}{r}\rho\int_0^\infty xdx\int_{|r-x|}^{|r+x|} ydyf^2(x)f^2(y) \times\sum_{\text{cyc}}\sum_{\sigma_3\tau_3}U\times(T(m_\pi x)T(m_\pi y))^2. \tag{27c}$$

In the above equations $P_2(x)$ are the usual Legendre polynomials. The z axis is taken along the vector $\mathbf{r}_{12}$ and the following definitions and abbreviations are also used:

$$\mathbf{r}_{12} = \mathbf{r}_{13}+\mathbf{r}_{32},\ x = |\mathbf{r}_{13}|,\ y = |\mathbf{r}_{32}|,\ r = |\mathbf{r}_{12}|, \tag{28}$$

$$\cos\theta_x = \hat{\mathbf{r}}_{12}.\hat{\mathbf{r}}_{23},\ \cos\theta_y = \hat{\mathbf{r}}_{12}.\hat{\mathbf{r}}_{13},\ \cos\theta = \hat{\mathbf{r}}_{13}.\hat{\mathbf{r}}_{23}, \tag{29}$$

$$P = -\tfrac{3}{2}\cos\theta(\cos\theta+3\cos\theta_x\cos\theta_y) - P_2(\cos\theta_y) - P_2(\cos\theta_x). \tag{30}$$

To calculate Eq. (25) three different scenarios for two-body correlation functions are considered in this work which are explained in the following. In the LOCV approach, two-body correlation functions can be extracted for each two-body channel. Since S waves have the most contributions to the wave function at short distances, it is a good approximation to determine $\bar{V}_{12}(r)$ by using only the $^1S_0$ channel two-body correlation function. Therefore we have applied this approximation as the first scenario for determining the effective

two-body potential. Then we go beyond this approximation in order to understand the effect of other two-body channels on $\bar{V}_{12}(r)$. To do this task we insert a state-averaged two-body correlation function in Eq. (25) which is defined as [37]

$$\bar{f}^2(r) = \frac{\sum_{\alpha,i}(2T+1)(2J+1)\frac{1}{2}[1-(-1)^{L+S+T}]f_\alpha^{(i)^2}a_\alpha^{(i)^2}(k_F r)}{\sum_{\alpha,i}(2T+1)(2J+1)\frac{1}{2}[1-(-1)^{L+S+T}]a_\alpha^{(i)^2}(k_F r)}, \tag{31}$$

where $a_\alpha^{(i)^2}(k_F r)$ come from summing over the plane-wave states and are written as

$$a_\alpha^{(1)^2}(x) \equiv x^2 I_L(x), \tag{32a}$$

$$a_\alpha^{(2)^2}(x) \equiv x^2(2J+1)^{-1}[(J+1)I_{J-1}(x) + J I_{J+1}(x)], \tag{32b}$$

$$a_\alpha^{(3)^2}(x) \equiv x^2(2J+1)^{-1}[J I_{J-1}(x) + (J+1)I_{J+1}(x)], \tag{32c}$$

where

$$I_J(x) \equiv 48\int_0^1 dz z^2\left(1-\frac{3}{2}z+\frac{1}{2}z^3\right)J_J^2(xz). \tag{33}$$

In this case, the resulting effective two-body force is noted by $\bar{V}_{12}^{av}(r)$. To be more precise, as the third scenario, we first put $\bar{f}(r)$ in Eq. (25) and use the resulting effective two-body force in the LOCV procedure. By doing this process, a so-called effective two-body correlation function is obtained. Then again we insert the mentioned effective two-body correlation function in Eq. (25) and repeat this iteration process till the convergence is reached. The final obtained effective two-body correlation function and the corresponding effective two-body potential are noted by $\bar{f}_{\rm it}(r)$ and $\bar{V}_{12}^{\rm it}(r)$, respectively.

In the next section we present our results regarding three mentioned types of effective two-body potentials and the effect of using TBF on the EOS of asymmetric nuclear matter and β-stable matter as well as the neutron star structure using different two-body interactions.

IV. RESULTS AND DISCUSSION

We begin presenting our results by providing those of effective two-body potential. As we mentioned in the previous section, one can reach three different values for effective two-body force depending on using $f(r)$, $\bar{f}(r)$, or $\bar{f}_{\rm it}(r)$ in Eq. (25) which are noted by $\bar{V}_{12}(r)$, $\bar{V}_{12}^{\rm av}(r)$, and $\bar{V}_{12}^{\rm it}(r)$, respectively. Three mentioned types of two-body correlation functions are shown in panel (a) of Fig. 1 for symmetric nuclear matter at $\rho_B = 0.17\,{\rm fm}^{-3}$ using the AV18 potential as the bare two-body interaction. It is seen that there is no significant difference between the values of $\bar{f}(r)$ and $\bar{f}_{\rm it}(r)$ at each given density while $f(r)$ has larger values compared to other two correlaton functions particularly at short distances. In panel (b) of this figure three components of corresponding two-body effective potentials, namely Eqs. (27a) to (27c), are plotted. It is seen that the absolute value of $\bar{V}_{12}(r)$ is slightly larger than other two effective two-body potentials since its corresponding correlation function, i.e., $f(r)$, has an overshoot at short distances [see panel (a) of this figure]. it can also be concluded from this panel that using different two-body correlation functions in Eq. (25) affects mostly the repulsive component of the resulting effective two-body force more than the other two components. The effect of increasing the baryon density on the $V_{\sigma\tau}^{2\pi}$, $V_t^{2\pi}$, and V_c^R components of the effective two-body force are shown in Figs. 2, 3, and 4, respectively. It can be seen that increasing the baryon density

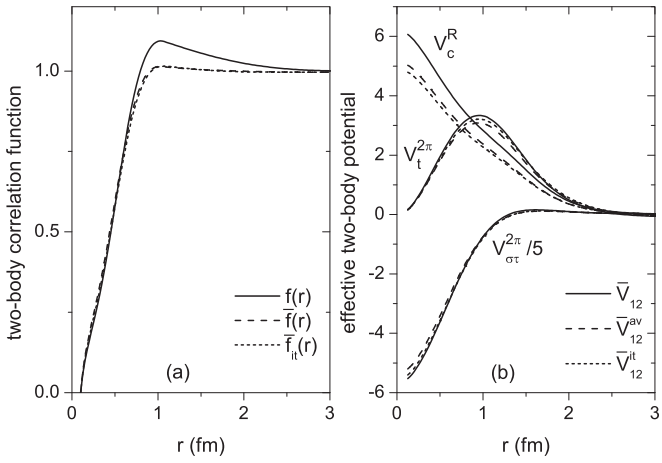

FIG. 1. (a) Three different types of two-body correlation functions mentioned in the text at $\rho_B = 0.17\,{\rm fm}^{-3}$ using the AV18 potential for SNM. (b) Components of three different types of effective two-body potentials corresponding to panel (a) correlation functions.

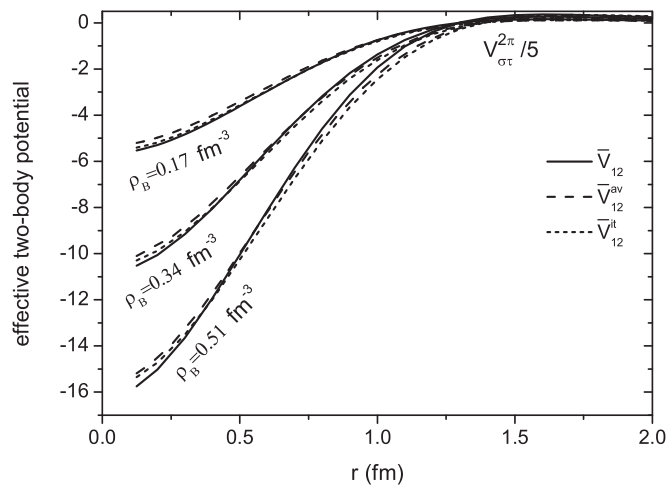

FIG. 2. $V_{\sigma\tau}^{2\pi}$ Component for three types of effective two-body potentials at different baryon densities using AV18 potential for SNM.

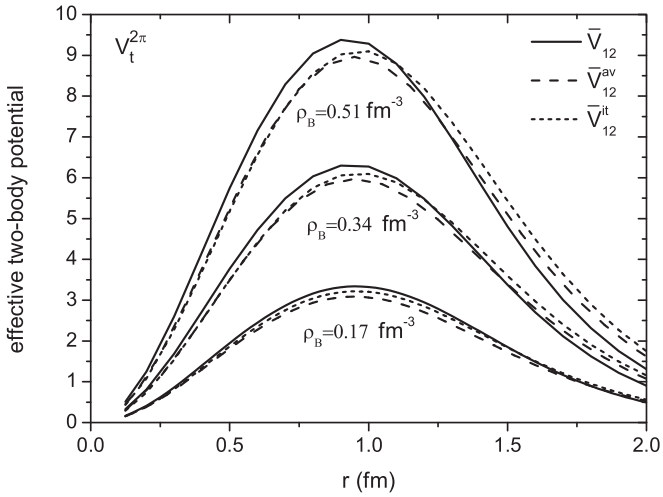

FIG. 3. Same as Fig. 2 but for the $V_t^{2\pi}$ component.

will result in increasing the absolute value of all three types of effective two-body potentials, as is expected. Moreover, as the density increases, the values of the $V_{\sigma\tau}^{2\pi}$ and $V_t^{2\pi}$ components of all three types of effective two-body potentials are more or less close to each other while the repulsive component V_c^R of $\bar{V}_{12}^{av}(r)$ and $\bar{V}_{12}^{it}(r)$ becomes smaller than those of $\bar{V}_{12}(r)$. As a result the EOS obtained by using $\bar{V}_{12}(r)$ is slightly stiffer at high densities compared to those obtained by either $\bar{V}_{12}^{av}(r)$ or $\bar{V}_{12}^{it}(r)$. On the other hand, since these differences occur mainly at short distances, namely less than 0.5 fm, they do not have a great influence on the energy expectation value. Therefore one can conclude that the approximation of using only the $^1S_0$ channel correlation function for obtaining the effective two-body potential is still a good one as other authors used it in their calculations [8,38]. The values of parameters A and U, which are adjusted in order to reproduce the correct saturation point in each individual mentioned cases, are listed in Table I. Results of the BHF approach for these two parameters [8] are also presented in this table for comparison.

TABLE I. The values of parameters A and U in the LOCV method (this work) as well as the BHF approach [8].

Potential	Method	A (MeV)	U (MeV)
AV18 + $\bar{V}_{12}$	LOCV	−0.041	0.000 523
AV + $\bar{V}_{12}^{av}$	LOCV	−0.048	0.000 514
AV18 + $\bar{V}_{12}^{it}$	LOCV	−0.051	0.000 512
AV18 + UIX	BHF [8]	−0.050	0.000 42

In Fig. 5 we have shown the effect of using the mentioned effective two-body forces on the EOS of symmetric nuclear matter. The AV18 potential is used as the bare two-body interaction in this comparison. As we have already concluded from previous figures, there is no significant difference between equations of state if one uses $\bar{V}_{12}^{av}(r)$ or $\bar{V}_{12}^{it}(r)$ in the Hamiltonian, since both effective two-body forces have approximately the same value at each baryon density. While $\bar{V}_{12}(r)$ is more repulsive compared to other mentioned effective two-body forces, the resulting EOS is correspondingly stiffer and as the baryon density increases, this difference becomes clearer. However, this difference is still quite small so that one can neglect the effect of other two-body channels in calculating the effective two-body force. Therefore $\bar{V}_{12}(r)$ is used as the effective two-body force in obtaining the following results. The EOS calculated without using TBF is also plotted in this figure. As we expected, adding TBF to the nuclear Hamiltonian makes the EOS much stiffer compared to that obtained by using only the AV18 potential and also shifts the saturation density toward lower densities. These results are in agreement with those obtained by other many-body methods [11,39,40].

Equations of state of symmetric nuclear matter determined by using different two-body potentials supplemented by a UIX three-body force are presented in panel (a) of Fig. 6. It is seen that by adding TBF to the nuclear Hamiltonian the empirical saturation point of the nuclear matter ($\rho_0 = 0.17 \pm 1\,\text{fm}^{-3}$ and $E_0/A = -16 \pm 1\,\text{MeV}$) is correctly reproduced for all used two-body forces. Therefore to reproduce the empirical

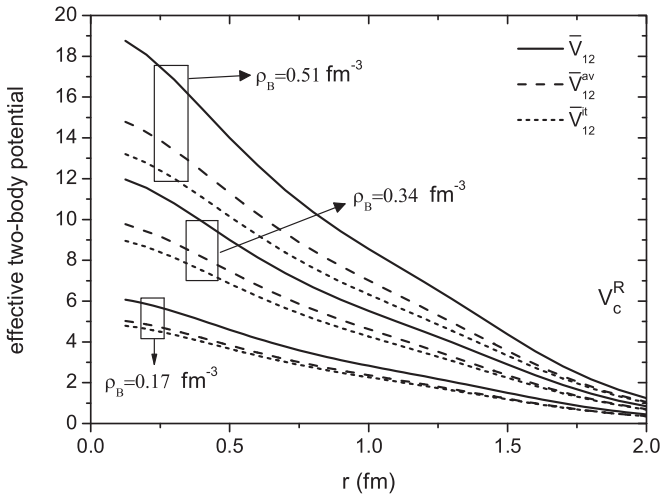

FIG. 4. Same as Fig. 2 but for the V_c^R component.

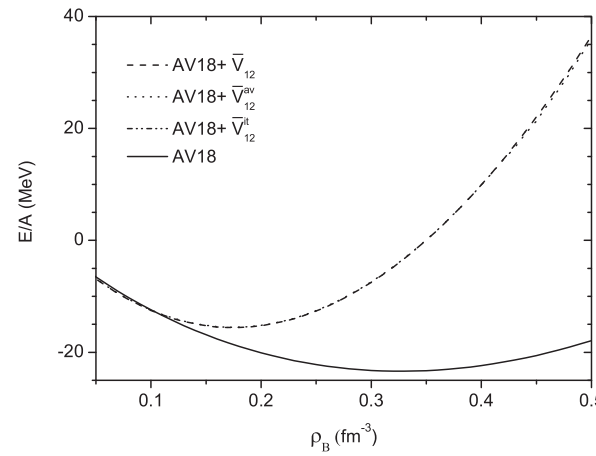

FIG. 5. Equation of state of symmetric nuclear matter using different effective two-body forces as well as using only the AV18 potential.

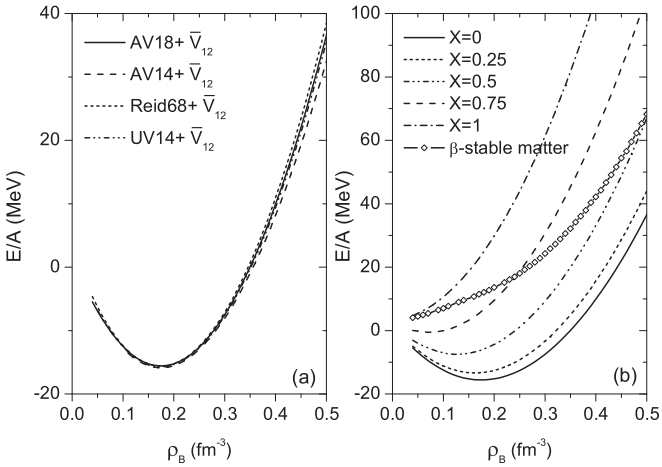

FIG. 6. (a) EOS of symmetric nuclear matter for different two-body potentials supplemented by TBF. (b) EOS of asymmetric nuclear matter for a number of asymmetry parameter X as well as β-stable matter using AV18 + $\bar{V}_{12}$ potential.

saturation point for each two-body interaction, an appropriate effective two-body force is first introduced by a self-consistent procedure using two-body correlation functions that come from the given two-body potential. Parameters A and U in the TBF are then changed until the empirical saturation point is reproduced correctly. Our results for saturation points with and without using TBF are listed in Table II.

It is also seen that in the low-density region the effect of TBF on the EOS is quite the same for all two-body potentials while at relatively high density this force provides different repulsive contributions to the EOS depending on the bare two-body interaction. This behavior is due to the fact that correlation functions that come from different two-body potentials do not have the same density dependence. However, because of the density-dependent nature of the UIX three-body force, the repulsion from this interaction becomes stronger for each individual EOS by increasing the baryon density. In panel (b) of Fig. 6 the EOS of asymmetric nuclear matter using the $AV18 + \bar{V}_{12}$ interaction is plotted for a number of asymmetric parameters $X = (\rho_n - \rho_p)/\rho_B$ from symmetric nuclear matter ($X = 0$) to pure neutron matter ($X = 1$). The EOS of β-stable matter is also presented in this panel. It is seen that, as is expected, by increasing the number of neutrons in the system the effective "potential well" becomes more shallow so that the system is no longer bound beyond a specific asymmetry parameter X_b. We have found $X_b = 0.771$ for AV18+TBF model and $X_b = 0.839$ in the case of using only AV18 potential. By comparing these two values one can conclude that TBF causes the bound system to occur at lower asymmetry parameter. These values are comparable with those obtained by the BHF approach [41]. It is also seen that as the asymmetry parameter increases the saturation point of bound systems shifts toward lower densities.

TABLE II. Saturation density ρ_0 and saturation energy E_0/A of symmetric nuclear matter using different potentials with and without TBF.

potential	ρ_0(fm^{-3})	E_0/A(MeV)
AV18	0.32	−23.37
AV14	0.3	−19.78
UV14	0.38	−16.08
Reid68	0.29	−22.83
AV18 + $\bar{V}_{12}$	0.1748	−15.58
AV14 + $\bar{V}_{12}$	0.1742	−15.88
UV14 + $\bar{V}_{12}$	0.1741	−15.70
Reid68 + $\bar{V}_{12}$	0.1742	−15.61

Another important quantity which plays a crucial role in understanding different physical and astrophysical issues is the nuclear symmetry energy (NSE) which is defined as

$$E_{\rm sym}(\rho) = \frac{1}{2}\frac{\partial^2 E(\rho, X)}{\partial X^2}\bigg|_{X=0.} \tag{34}$$

Despite of both experimental and theoretical efforts in determining the NSE, its value at normal density is still uncertain and the density dependence of this quantity is poorly known particularly at supernormal densities. A liquid drop model calculation gives a result of 32.65 MeV for this quantity [42]. Moreover, an analysis of isovector giant dipole resonance (GDR) data within relativistic mean-field (RMF) theory set a range of $34 \leqslant E_{\rm sym} \leqslant 36$ MeV [43]. The density dependence of $E_{\rm sym}$ predicted by LOCV calculations is presented in Fig. 7 as well as the results of some other many-body approaches such as BHF [7,44,45], variational [11], and DBHF [46,47] models. The effect of the inclusion of TBF is also shown in this figure. It is seen that using TBF in nonrelativistic methods leads to a repulsive contribution to the symmetry energy and consequently to a stiffening of the density dependence of this quantity. This effect becomes much stronger at high densities. Although the NSE predicted by all models and potentials is an increasing function of density, the density dependence of $E_{\rm sym}$

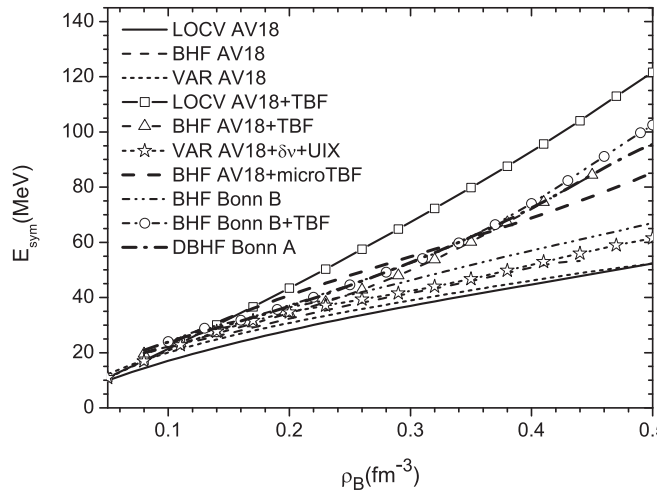

FIG. 7. Density dependence of the nuclear symmetry energy obtained by the LOCV approach as well as some other many-body techniques such as BHF (with AV18, AV18+TBF, Bonn-B, Bonn B+TBF) [44,45], BHF (AV18+microTBF) [7], variational (AV18, AV18+δv+UIX) [11], and DBHF [46,47].

TABLE III. Approximate values of saturation density as well as binding energy per nucleon and symmetry energy at normal density for a number of many-body approaches with and without TBF.

Method	Potential	$\rho_0(\mathrm{fm}^{-3})$	E_0/A(MeV)	$E_{\mathrm{sym}}(\rho_0)$(MeV)
LOCV (This work)	AV18	0.32	−23.37	39.13
BHF [44,45]	AV18	0.26	−18.2	38.15
Variational [11]	AV18	0.3	−18.23	38.86
LOCV (This work)	AV18+TBF	0.1748	−15.58	37.51
BHF [44,45]	AV18+TBF	0.19	−15.2	33.48
Variational [11]	AV18+$\delta\upsilon$+UIX	0.186	−12.37	33.34
BHF [7]	AV18+microTBF	0.17	−15.5	36.03
BHF [44,45]	Bonn B	0.34	−22.07	50.68
BHF [44,45]	Bonn B+TBF	0.17	−15.87	32.9
DBHF [46]	Bonn A(complete $p\upsilon$)	0.193	−16.9	36.74
DBHF [46]	Bonn A(subtracted T-matrix)	0.1814	−16.3	34.36

from each approach is quite different at high densities. The values of saturation density as well as the binding energy per nucleon and E_{sym} at normal density are reported in Table III. The approximate values of mentioned quantities obtained within other approaches are also presented in this table. In the case of the inclusion of the TBF, the saturation density and binding energy per nucleon predicted by the LOCV model is in agreement with the empirical saturation point although the value of nuclear symmetry energy at normal density is high since the EOS obtained by the LOCV model is generally stiff. High value of NSE can also be seen in the results of other approaches such as the DBHF calculation with Bonn-A potential [46]. It is also seen that in some models, although the value of NSE is in agreement with the experimental results, either the saturation density or the binding energy is not in the proper range. For example see the results of the variational approach [11].

In order to understand the effect of using TBF on the neutron star structure, one should study the role played by this force in the EOS of NS matter. For determining neutron star gravitational mass as a function of radius and central energy density, one can use the Tolman-Openheimer-Volkoff (TOV) equations [48] which are written as

$$\frac{dP(r)}{dr} = -\frac{GM(r)\varepsilon(r)}{c^2r^2}\left(1+\frac{P(r)}{\varepsilon(r)}\right)\left(1+\frac{4\pi r^3P(r)}{M(r)c^2}\right) \times \left(1-\frac{2GM(r)}{rc^2}\right)^{-1}, \quad (35)$$

$$\frac{dM(r)}{dr} = \frac{4\pi\varepsilon(r)r^2}{c^2}. \quad (36)$$

In the above relations $P(r)$, $\varepsilon(r)$, and $M(r)$ denote the pressure, mass-energy density of the NS matter (which is defined as the total energy of the system plus the rest mass of involved particles), and the enclosed gravitational mass, respectively. G is the gravitational constant. Starting with a central mass-energy density ε_c, calculations are done until we reach zero pressure that indicates the surface of the neutron star.

In this work we model the NS by β-stable matter. Panel (a) of Fig. 8 displays the mass-energy $[\varepsilon(r)\rho_B]$ of β-stable matter as a function of baryon density with and without TBF for two two-body potentials, namely AV18 and AV14. It is clearly seen that the repulsive term in the TBF dominates at high-density region and results in increasing the stiffness of the EOS and correspondingly in increasing the maximum gravitational mass of the star. In panel (b) of this figure the pressure of β-stable matter is plotted using different two-body interactions combined with TBF. Results presented in this figure are then used in Eq. (35) for determining the structure of neutron stars.

Figure 9 displays particle fractions x_i for β-stable matter as a function of baryon density. In panel (a) of this figure, the LOCV results of the proton fraction and electron fraction as well as muon fraction are presented using the AV18 potential with and without TBF. It is seen that particle fractions obtained from the AV18+TBF calculation have, in general, larger values but the same behavior compared to those calculated by using only the AV18 interaction. It is also seen that using TBF causes muons to appear at lower densities compared to the case where no TBF is used in the Hamiltonian. In our model muons start to appear at $\rho \sim 0.12\,\mathrm{fm}^{-3}$ if TBF is used and at $\rho \sim 0.17\,\mathrm{fm}^{-3}$ if TBF is not included. Figure 9(b) shows a comparison between the results for proton fraction x_p obtained by the LOCV approach and those provided by other many-body methods and three-body forces, namely the variational chain summation methods by APR (AV18+UIX) [11] and WFF

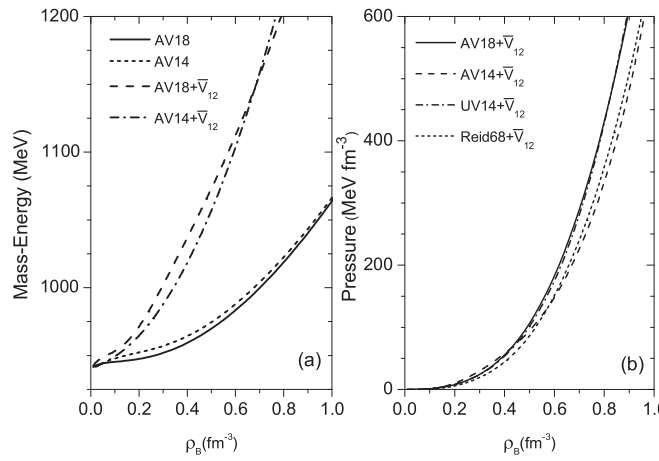

FIG. 8. (a) Mass-energy and (b) pressure of β-stable matter using different potentials.

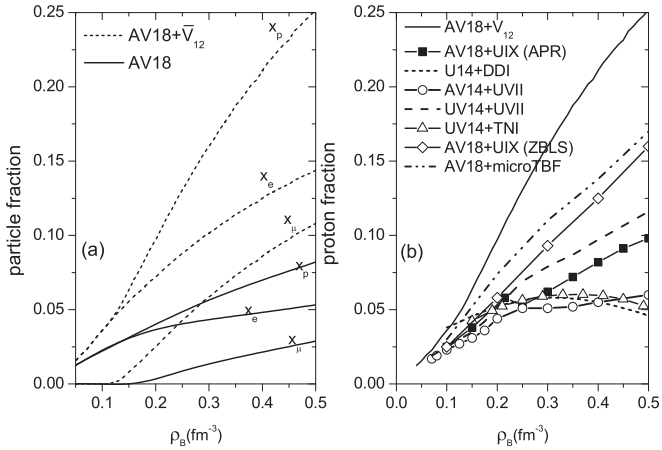

FIG. 9. (a) Proton, electron, and muon fractions for β-stable matter against baryon density with and without TBF using the AV18 potential. (b) Comparison of proton fraction obtained in the present work (black solid curve) with the results of AV18+UIX (APR) [11], AV14+UVII [40], UV14+UVII [40], UV14+TNI [40], U14-DDI [43], AV18+UIX (ZBLS) [7], and AV18+microTBF [7].

(AV14+UVII, UV14+UVII and UV14+TNI models) [40], the U14-DDI model [49] and BHF method (using AV18+UIX and AV18+microTBF potentials)[7]. A saturation in x_p can be seen in some calculations such as UV14+TNI and U14+DDI while the proton fraction shows the same general behavior as the results of our approach in other models.

To ensure the relativistic causality condition in such matter, we have plotted in Fig. 10 the speed of sound which is given by the following relation:

$$\frac{c_s}{c} = \left(\frac{dP}{d\varepsilon}\right)^{\frac{1}{2}}. \tag{37}$$

In this figure c_s is plotted in units of the speed of light c as a function of density up to the central density which corresponds to the maximum mass of a neutron star using the AV18 potential with and without TBF. It is seen that in both

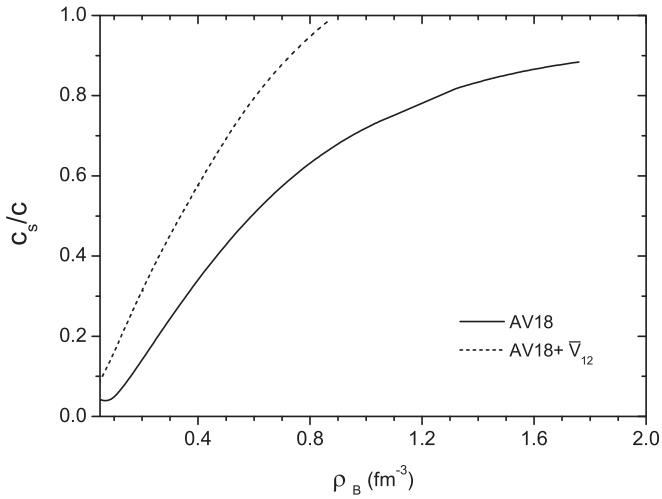

FIG. 10. Speed of sound as a function of baryon density for β-stable matter with and without TBF.

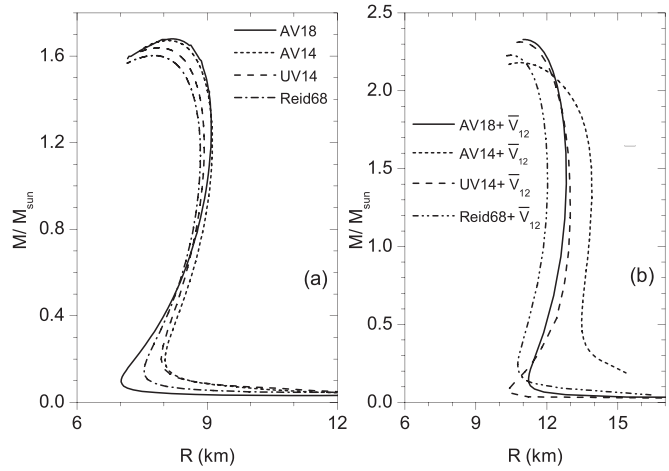

FIG. 11. Mass-radius relation of neutron star with (b) and without (a) TBF using different two-body potentials.

cases the speed of sound does not exceed that of light through whole density range that NS is stable.

Now we are in the position of presenting our results regarding the neutron star structure. The gravitational mass of the NS in the unit of solar mass is plotted in Fig. 11 as a function of radius for different two-body potentials with [panel (a)] and without [panel (b)] TBF. The exact values of maximum masses are reported in Table IV. This table also includes approximate values for maximum masses obtained by other many-body models for comparison. In general, as we expected, the equation of sates calculated by using TBF produce larger gravitational masses compared to those obtained by using only two-body forces. More precisely, as can be seen in Fig.11(a) calculations based on only two-body interactions result in maximum masses below 1.8 $M_\odot$, while the models containing

TABLE IV. Comparison of maximum masses obtained in the present work with those calculated within other many-body approaches.

Potential	Method	Author	$M/M_\odot$
BOB + microTBF	BHF	LS [8]	2.5
AV18 + microTBF	BHF	LS [8]	2.3
$N93$ + microTBF	BHF	LS [8]	2.12
AV18 + UIX	BHF	LS [8]	1.8
AV18 + UIX	Varitional	APR [11]	2.38
AV18	Varitional	APR [11]	1.67
UV14 + UVII	Varitional	WFF [40]	2.19
AV14 + UVII	Varitional	WFF [40]	2.13
UV14 + TNI	Varitional	WFF [40]	1.84
AV18	LOCV	This work	1.68
AV14	LOCV	This work	1.67
UV14	LOCV	This work	1.64
Reid68	LOCV	This work	1.60
AV18 + UIX	LOCV	This work	2.33
AV14 + UIX	LOCV	This work	2.18
UV14 + UIX	LOCV	This work	2.31
Reid68 + UIX	LOCV	This work	2.23

TBF have maximum masses above $2M_\odot$. Equations of state which provide maximum masses above $2M_\odot$ are able to predict the existence of a $M = 2.01 \pm 0.04 M_\odot$ neutron star which has been recently reported [4] and therefore are in good agreement with empirical observations. Moreover, from panel (b) of this figure it can be seen that radii of neutron stars modelled by using TBF are close to or in the proper range that is determined by recent analysis [5,6].

V. CONCLUSION

In conclusion we have improved the LOCV approach by using a three-nucleon potential in this formalism and have shown that by adding TBF to our nuclear Hamiltonian, this method is able to reproduce the correct saturation point of symmetric nuclear matter. We have calculated the effective two-body force by using different two-body correlation functions and have shown that the approximation of using only the $^1S_0$ channel correlation function for determining the effective two-body potential is an acceptable one. We have also shown that using TBF results increases the maximum gravitational mass of neutron stars compared to that determined without using TBF so that results we obtained for maximum mass and the corresponding radius of neutron stars are in acceptable agreement with recently reported empirical values.

ACKNOWLEDGMENTS

We would like to thank the Research Council of University of Tehran for the grants provided for us.

[1] H. A. Bethe, Rev. Mod. Phys. **62**, 801 (1990).
[2] S. L. Shapiro and S. A. Teukolsky, *Black Holes, White Dwarfs and Neutron Stars* (John Wiley & Sons, New York, 1983).
[3] P. Demorest, T. Pennucci, S. Ransom, M. Roberts, and J. Hessels, Nature (London) **467**, 1081 (2010).
[4] J. Antoniadis *et al.*, Science **340**, 6131 (2013).
[5] J. M. Lattimer and A. W. Steiner, Astrophys. J. **784**, 123 (2014).
[6] J. M. Lattimer and A. W. Steiner, Eur. Phys. J. A **50**, 40 (2014).
[7] X. R. Zhou, G. F. Burgio, U. Lombardo, H.-J. Schulze, and W. Zuo, Phys. Rev. C **69**, 018801 (2004).
[8] Z. H. Li and H.-J. Schulze, Phys. Rev. C **78**, 028801 (2008).
[9] G. Q. Li, R. Machleidt, and R. Brockmann, Phys. Rev. C **45**, 2782 (1992); P. G. Krastev and F. Sammarruca, *ibid.* **74**, 025808 (2006).
[10] D. Alonso and F. Sammarruca, Phys. Rev. C **67**, 054301 (2003).
[11] A. Akmal, V. R. Pandharipande, and D. G. Ravenhall, Phys. Rev. C **58**, 1804 (1998).
[12] J. Morales, V. R. Pandharipande, and D. G. Ravenhall, Phys. Rev. C **66**, 054308 (2002).
[13] B. S. Pudliner, V. R. Pandharipande, J. Carlson, and R. B. Wiringa, Phys. Rev. Lett. **74**, 4396 (1995); B. S. Pudliner, V. R. Pandharipande, J. Carlson, S. C. Pieper, and R. B. Wiringa, Phys. Rev. C **56**, 1720 (1997).
[14] S. Gandolfi, F. S. Pederiva, S. Fantoni, and K. E. Schmidt, Phys. Rev. C **73**, 044304 (2006).
[15] M. Pervin, S. C. Pieper, and R. B. Wiringa, Phys. Rev. C **76**, 064319 (2007).
[16] J. C. Owen, R. F. Bishop, and J. M. Irvine, Phys. Lett. B **59**, 1 (1975).
[17] M. Modarres and J. M. Irvine, J. Phys. G: Nucl. Part. Phys. **5**, 511 (1979).
[18] R. V. Reid, Ann. Phys. (NY) **50**, 411 (1968).
[19] A. M. Green, J. A. Niskanen, and M. E. Sainio, J. Phys. G: Nucl. Part. Phys. **4**, 1055 (1978).
[20] H. R. Moshfegh and M. Modarres, Nucl. Phys. A **759**, 79 (2005).
[21] H. R. Moshfegh and M. Modarres, Nucl. Phys. A **792**, 201 (2007).
[22] M. Modarres, J. Phys. G: Nucl. Part. Phys. **19**, 1349 (1993).
[23] M. Modarres, J. Phys. G: Nucl. Part. Phys. **21**, 351 (1995).
[24] M. Modarres and H. R. Moshfegh, Phys. Rev. C **62**, 044308 (2000); Prog. Theor. Phys. **107**, 139 (2002).
[25] G. H. Bordbar and M. Modarres, J. Phys. G: Nucl. Part. Phys. **23**, 1631 (1998); Phys. Rev. C **57**, 714 (1998); M. Modarres and G. H. Bordbar, *ibid.* **58**, 2781 (1998).
[26] R. B. Wiringa, R. A. Smith, and T. L. Ainsworth, Phys. Rev. C **29**, 1207 (1984).
[27] R. B. Wiringa, V. G. J. Stoks, and R. Schiavilla, Phys. Rev. C **51**, 38 (1995).
[28] I. E. Lagaris and V. R. Pandharipande, Nucl. Phys. A **359**, 331 (1981).
[29] S. Zaryouni and H. R. Moshfegh, Eur. Phys. J. A **45**, 69 (2010).
[30] S. Zaryouni, M. Hassani, and H. R. Moshfegh, Phys. Rev. C **89**, 014332 (2014).
[31] M. Modarres, A. Rajabi, and H. R. Moshfegh, Phys. Rev. C **76**, 064311 (2007).
[32] M. Modarres, H. R. Moshfegh, and K. Fallahi, Eur. Phys. J. B **36**, 485 (2003).
[33] S. C. Pieper, V. R. Pandharipande, R. B. Wiringa, and J. Carlson, Phys. Rev. C **64**, 014001 (2001).
[34] J. W. Clark, Prog. Part. Nucl. Phys. **2**, 89 (1979).
[35] M. Modarres and J. M. Irvine, J. Phys. G: Nucl. Part. Phys. **5**, 7 (1979).
[36] P. Grangé, A. Lejeune, M. Martzolff, and J.-F. Mathiot, Phys. Rev. C **40**, 1040 (1989).
[37] M. Modarres and J. M. Irvine, J. Phys. G: Nucl. Part. Phys. **5**, 1 (1979).
[38] M. Baldo and L. S. Ferreira, Phys. Rev. C **59**, 682 (1999).
[39] M. Baldo and H. R. Moshfegh, Phys. Rev. C **86**, 024306 (2012).
[40] R. B. Wiringa, V. Fiks, and A. Fabrocini, Phys. Rev. C **38**, 1010 (1988).
[41] Zuo Wei, A. Lejeune, U. Lombardo, and J. F. Mathiot, Commun. Theor. Phys. **39**, 439 (2003).
[42] W. D. Myers and W. J. Swiatecky, Nucl. Phys. A **601**, 141 (1996).
[43] T. Niksic, D. Vretenar, and P. Ring, Phys. Rev. C **66**, 064302 (2002).
[44] W. Zuo, A. Lejeune, U. Lombardo, and J. F. Mathiot, Nucl. Phys. A **706**, 418 (2002).
[45] Z. H. Li, U. Lombardo, H.-J. Schulze, and W. Zuo, Phys. Rev. C **77**, 034316 (2008).

[46] E. N. E. van Dalen, C. Fuchs, and A. Faessler, Nucl. Phys. A **744**, 227 (2004).
[47] E. N. E. van Dalen, C. Fuchs, and A. Faessler, Phys. Rev. C **72**, 065803 (2005).
[48] J. Oppenheimer and G. Volkoff, Phys. Rev. **55**, 374 (1939).
[49] C. P. Lorenz, D. G. Ravenhall, and C. J. Pethick, Phys. Rev. Lett. **70**, 379 (1993).